



# Novel 2D strain-rate-dependent lamina-based and RVE/phase-based progressive fatigue damage criteria for randomly loaded multi-layer fiber-reinforced composites

M. Shariyat

Faculty of Mechanical Engineering, K.N. Toosi University of Technology, Tehran, Iran.

shariyat@kntu.ac.ir

**ABSTRACT.** Two implicit progressive fatigue damage models that rely on new equivalent-damage and equivalent-stress criteria are presented for the prediction of various failure modes of the composites. The criteria are coupled with lamina-based and representative-volume-element-based damage progression approaches. The common concepts of residual strength and residual stiffness are revisited and modified. A fatigue life assessment algorithm that incorporates the strain-rate-dependence of the fatigue strengths and stiffnesses, and random and asynchronous changes of the stress components, distinct mean values, and phase shifts of the stress components is employed. New ideas and new post-processing procedures are employed in the current research. It is the first time that the significant impacts of the strain-rate-dependence of the properties of the composites on stress and fatigue life analyses are investigated. Results of the proposed fatigue criteria are first implemented to a composite plate with a complex lamination scheme under a random transverse load and the predicted fatigue lives are verified by the experimental results. Then, these criteria are implemented to a composite chassis frame of an SUV car under realistic random road inputs and the theoretical results are verified by the experimental results. Results confirm the significant role of the strain-rate-dependence effects on the fatigue lives.

**KEYWORDS.** HCF progressive damage criteria; Fiber-reinforced composites; Strain-rate effects; RVE-based approach; Experimental results.



**Citation:** Shariyat, M., Novel 2D strain-rate-dependent lamina-based and RVE/phase-based progressive fatigue damage criteria for randomly loaded multi-layer fiber-reinforced composites, *Frattura ed Integrità Strutturale*, 59 (2022) 423-443.

**Received:** 19.11.2021

**Accepted:** 28.11.2021

**Published:** 01.01.2021

**Copyright:** © 2022 This is an open access article under the terms of the CC-BY 4.0, which permits unrestricted use, distribution, and reproduction in any medium, provided the original author and source are credited.

## INTRODUCTION

Modern composites have been used extensively in durable and ultra-safe engineering structures. The range of their usage includes the hi-tech structures, e.g., infrastructures of the astronautics, aeronautics, and hovercraft infrastructures to the common applications. The fiber-reinforced composites are vulnerable to various failure modes such as matrix/fiber breakage or cracking, fiber slippage relative to the matrix, debonding, and delamination.



During the past years, various approaches have been adopted for fatigue analysis of composites. Zhang et al. [1] developed a fatigue damage model based on a Tsai–Hill-type effective stress for orthotropic materials. Some researchers proposed some progressive damage models or used the residual strength concept. Lian and Yao [2] employed a Hashin-type criterion that considered the degradations in the stiffness and strength of the material. Multiaxial fatigue analysis was conducted by Quaresimin et al. [3] to consider the effects of the bidirectional load ratio.

Fewer researches have taken into account the influence of the stress ratio on the fatigue analysis results. Nyman [4] utilized a Tsai–Hill-type criterion to present fatigue failure functions based on an available S-N curve for a multi-directional composite. The influence of the stress ratio was incorporated through a Goodman-type correction technique. Considering the sudden and gradual logics of material properties degradation, Naderi and Maligno [5] and developed a finite element progressive fatigue damage model for carbon/epoxy composite laminates with different layup sequences. Dong et al. [6] as well used the same residual strength and material properties degradation models and material but employed Puck's failure theory instead, for multidirectional composite laminates with arbitrary stacking sequences. Passipoularidis et al. [7] presented a progressive damage fatigue modeling algorithm in ply level for variable-amplitude loads, utilizing Puck's failure criterion, residual strength, and gradual/sudden stiffness degradation methodologies. Carrella-Payan et al. [8] simulated the intra-laminar fatigue damage in unidirectional composites under multi-axial and variable amplitude loadings, using a stiffness degradation law and the damage cycle jump concept that was implemented into Siemens PLM commercial software. Yang et al. [9] presented a short review on the phenomenological and progressive damage models of the fatigue life prediction of the fiber-reinforced ceramic-matrix composites under, thermomechanical loadings. They concluded that progressive damage models are the most effective models. Recently, Vassilopoulos [10] reviewed the evolution of the fatigue life assessment theories of the fiber-reinforced composites with a special focus on parameters that affect the S-N curves of the composite materials.

The current article is concerned with the suggestion of new ideas for the development of two categories, i.e., lamina-based and phase-based, progressive-damage fatigue life assessment criteria that can be employed for composites with arbitrary lamination schemes under loads with arbitrary time-variations patterns. New ideas are presented for tracing the damage progression phenomenon, various types of failure, cyclic degradation in the elastic modulus, and strain-rate-dependence of the material properties and fatigue strengths. Some of the critical points that distinguish the present work from those accomplished so far are:

- Inherently different ideas are introduced and utilized for the suggestion of two kinds of failure-type-based fatigue criteria.
- The proposed criteria have been developed based on two distinct: (1) damage-based, and (2) equivalent-stress-based frameworks.
- The criteria may be employed for the prediction of the various failure modes.
- The proposed fatigue failure criteria are imposed on novel lamina-based and representative-volume-element (RVE)-based progressive fatigue damage models that use bridging laws utilizing the local stresses of the individual phases instead of the stress field of the mixture. While the introduced algorithm admits incorporation of the different ratios/means and phase-lags/leads of the resulting different stresses, it provides modified rules for evaluation of the accumulated fatigue damages.
- The common fatigue failure, residual strength, and material properties degradation concepts are discussed in-depth and modified.
- The degradation in the material properties and the progressive or switching phase damages can be traced by the introduced formulation and numerical scheme.
- The significant strain-rate-dependence of both the material properties and fatigue strengths is considered in the: (1) stress analysis and (2) fatigue life assessment, for the first time.
- The presented formulations and modeling procedures are applied to a composite chassis of a redesigned SUV under random loads and the predicted results are verified by the experiments conducted by the author.

## DEVELOPMENT OF TWO MORE GENERAL CATEGORIES OF THE HIGH CYCLE FATIGUE CRITERIA

**T**wo quite different frameworks are chosen to propose two new phase-failure-based fatigue damage models:

- (1) equivalent-damage-based
- (2) Equivalent-stress-based models.

Although a limited portion of the original ideas of these criteria has already been proposed by the author [11], the employed concepts, the modeling procedure (especially, the RVE-based one), and incorporation of the ideas of the strain-rate-



dependence of both the material properties and fatigue strengths (S-N and T-N curves) are novel and the life assessment algorithm is new.

#### *The equivalent-damage-based criterion*

The fatigue failure modes of the fiber-reinforced composites are inherently quite different from those of the isotropic materials; as these failures are usually direction-dependent and localized ones and may occur within each of the constituent phases or at the interfaces between the phases. Moreover, the fatigue strengths of the successive layers are not identical in composites (e.g., in a [(90,±45,0)2]s laminate).

The early static failure criterion Tsai-Wu criterion was presented for the static loadings:

$$F_i \sigma_i + F_{ij} \sigma_i \sigma_j = 1 \quad (1)$$

For orthotropic materials with three planes of symmetry parallel to the coordinate planes, this criterion becomes:

$$F_{11} \sigma_1^2 + F_{22} \sigma_2^2 + F_{66} \sigma_6^2 + 2F_{12} \sigma_1 \sigma_2 + F_1 \sigma_1 + F_2 \sigma_2 = 1 \quad (2)$$

where

$$\begin{aligned} F_{11} &= \frac{1}{X_t X_c}, & F_{22} &= \frac{1}{Y_t Y_c}, & F_{66} &= \frac{1}{S^2}, & F_1 &= \frac{1}{X_t} - \frac{1}{X_c}, \\ F_2 &= \frac{1}{Y_t} - \frac{1}{Y_c}, & F_{12} &= -\frac{1}{2} \sqrt{F_{11} F_{22}} \end{aligned} \quad (3)$$

where  $X$ ,  $Y$ , and  $S$  are respectively, the static strengths along the first and second principal axes and the shear strength of the material. Hashin imposed that criterion to the fiber and matrix phases individually to check the different types of damages of the composite:

$$\begin{cases} \frac{\sigma_1}{F_{11}} = 1 \\ \left( \frac{\sigma_2}{F_{22}} \right)^2 + \left( \frac{\sigma_4}{F_{44}} \right)^2 + \left( \frac{\sigma_6}{F_{66}} \right)^2 = 1 \\ \left( \frac{\sigma_3}{F_{33}} \right)^2 + \left( \frac{\sigma_4}{F_{44}} \right)^2 + \left( \frac{\sigma_5}{F_{55}} \right)^2 = 1 \end{cases} \quad (4)$$

Puck and Schurmann [12] used the bases of the Coulomb-Mohr criterion to propose a polynomial-type criterion in terms of the normal and shear stresses of the failure plane, using two different friction coefficients:

$$\left( \frac{\tau_T}{S_T - \mu_T \sigma_n} \right)^2 + \left( \frac{\tau_L}{S_L - \mu_L \sigma_n} \right)^2 = 1 \quad (5)$$

where  $\tau_T$ ,  $\tau_L$ ,  $\sigma_n$ ,  $\mu_T$ ,  $\mu_L$  and  $S_T$  and  $S_L$  are the longitudinal/transverse shear and normal stresses of the cross-sectional plane, friction coefficients, and shear strengths, respectively.

Generally, the fatigue strengths are functions of the elapsed cycles ( $N$ ), stress ratio, and the loading frequency:

$$F_{ij} = F_{ij}(N, R, f), \quad F_i = F_i(N, R, f), \quad S = S(N, R, f) \quad (6)$$

Therefore, based on the S-N curves, one may write:



$$X(N, R, f) = X_0 N^{-m_x^{-1}}, \quad Y(N, R, f) = Y_0 N^{-m_y^{-1}}, \quad S(N, R, f) = S_0 N^{-m_s^{-1}} \quad (7)$$

where  $m$  denotes slope of the curve in the log-log plane and  $X_0$  etc., resemble  $\sigma'_f$  of Basquin's equation. In the construction of the S-N curves, the tension-compression anisotropy is inherently incorporated. For this reason, one may rewrite Eqn. (3) as:

$$\begin{aligned} F_{11} &= \frac{1}{X^2(N, R, f)}, \quad F_{22} = \frac{1}{Y^2(N, R, f)}, \quad F_{66} = \frac{1}{S^2(N, R, f)}, \\ F_{12} &= \frac{1}{2X(N, R, f)Y(N, R, f)}, \quad F_1 = F_2 = 0 \end{aligned} \quad (8)$$

Therefore, according to the Tsai-Wu-based Vassilopoulos [10] model, Eqn. (2) becomes as follows for a specified R:

$$\left[ \frac{\sigma_1}{X(N_f)} \right]^2 + \left[ \frac{\sigma_2}{Y(N_f)} \right]^2 + \left[ \frac{\sigma_6}{S(N_f)} \right]^2 - \frac{\sigma_1 \sigma_2}{X(N_f)Y(N_f)} = 1 \quad (9)$$

Many modifications are still vital to achieve curate fatigue criteria. To start the modifications, first, Eqn. (9), is expressed by each of the following equations, to cover the nonproportional loading conditions as well:

$$\left[ \frac{\sigma_{a1}}{\Sigma_{a1}(n_{\sigma_1}, N_{\sigma_1}, R_{\sigma_1})} \right]^2 + \left[ \frac{\sigma_{a2}}{\Sigma_{a2}(n_{\sigma_2}, N_{\sigma_2}, R_{\sigma_2})} \right]^2 + \left[ \frac{(\tau_{12})_a}{T_a(n_{\tau}, N_{\tau}, R_{\tau})} \right]^2 - \frac{\sigma_{a1} \sigma_{a2}}{\Sigma_{a1}(n_{\sigma_1}, N_{\sigma_1}, R_{\sigma_1}) \Sigma_{a2}(n_{\sigma_2}, N_{\sigma_2}, R_{\sigma_2})} = 1 \quad (10)$$

where  $\Sigma$  and  $T$  stand for the tension-compression and shear fatigue strengths and the subscript  $a$  denotes the amplitude value. Since the number of cycles of the different stress components may not always be identical, different  $n$  values are assigned to the stress components in Eqn. (10). Moreover, the residual stiffness and strengths differ from a direction to another. Hence, the fatigue strength associated with each stress component may be interpreted as a function of the  $n$ ,  $N$ , and  $R$  parameters in the relevant direction. On the other hand:

$$R_{\sigma_1} \equiv R_{\sigma_1}(t); \quad R_{\sigma_2} \equiv R_{\sigma_2}(t); \quad R_{\tau} = R_{\tau}(t) \quad (11)$$

Namely, unlike the common assumption, the stress ratio R varies with time; so that, different values may be gained for different segments of the time history of each stress component. These variations may be described by piecewise-defined functions. Moreover, the numerators of Eqn. (10), i.e.,  $\sigma_{a1}$ ,  $\sigma_{a2}$ , and  $(\tau_{12})_a$  may be determined through applying an adequate cycle counting procedure, such as the Rain Flow technique on histograms of the stress components. Based on the constant life diagrams (CLDs), the fatigue strengths may be connected to that of  $R=-1$  as:

$$\Sigma_a(R_{\sigma}) = \Sigma_a(R = -1, n_{\sigma_1}, N_{\sigma_1}) \Gamma(\sigma_m, \sigma_u) \quad (12)$$

The  $\Gamma$  function may be determined based on an interpolation function or a neural network, e.g., according to the data reported by Passipoularidis et al. [7], Kawai and Yano [13], Mandell [14], Nijssen [15], Reis et al. [16], and DOE/MSU composite material fatigue database [17], for Carbon/Epoxy and Glass/Epoxy materials. Some typical variations of the fatigue stress amplitude versus the stress ratio (CLDs) are demonstrated in Fig. 1.

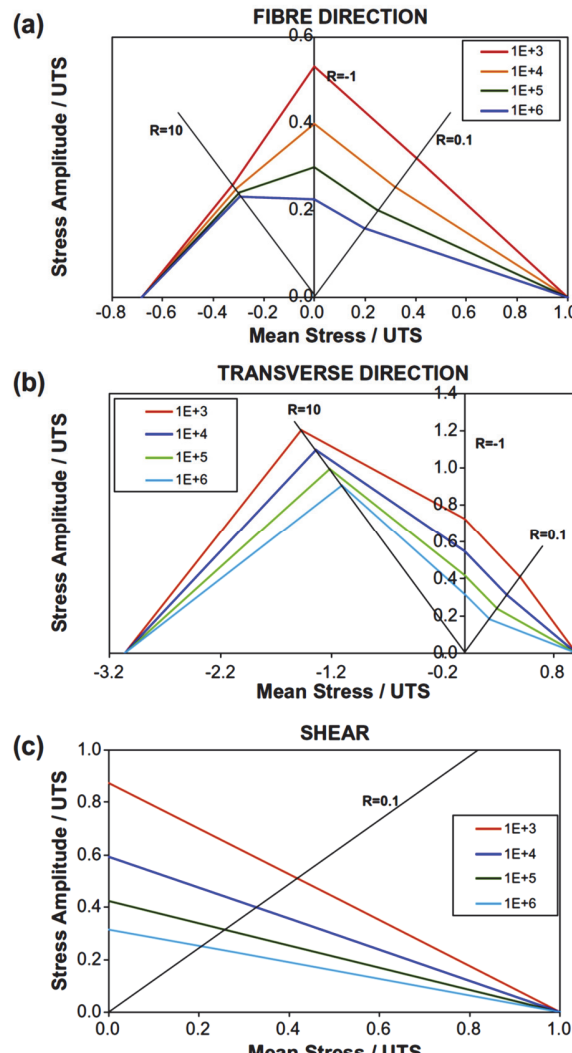


Figure 1: Samples (not used by the present research) of variations of the fatigue stress amplitude versus the mean stress (constant fatigue life diagrams), for a UD Glass/Epoxy ply [7]: (a) in the direction of fibers, (b) transverse to fibers, and (c) in-plane shear.

Based on Eqn. (12), Eqn. (10) becomes:

$$\begin{aligned}
& \left[ \frac{\sigma_{a1}}{\Sigma_{a1}(n_{\sigma_1}, N_{\sigma_1}) \Big|_{R_{\sigma_1}=-1} \Gamma_{\sigma_1}(\sigma_m, \sigma_u)} \right]^2 + \left[ \frac{\sigma_{a2}}{\Sigma_{a2}(n_{\sigma_2}, N_{\sigma_2}) \Big|_{R_{\sigma_2}=-1} \Gamma_{\sigma_2}(\sigma_m, \sigma_u)} \right]^2 + \\
& + \left[ \frac{(\tau_{12})_a}{T_a(n_{\tau}, N_{\tau}) \Big|_{R_{\tau}=-1} \Gamma_{\tau_{12}}(\tau_m, \tau_u)} \right]^2 + \\
& - \frac{\sigma_{a1}\sigma_{a2}}{\Sigma_{a1}(n_{\sigma_1}, N_{\sigma_1}) \Big|_{R_{\sigma_1}=-1} \Sigma_{a2}(n_{\sigma_2}, N_{\sigma_2}) \Big|_{R_{\sigma_2}=-1} \Gamma_{\sigma_1}(\sigma_m, \sigma_u) \Gamma_{\sigma_2}(\sigma_m, \sigma_u)} = 1
\end{aligned} \tag{13}$$

Indeed, using the  $\Gamma$  function is identical to imposing Puck and Schurmann (i.e., Coulomb-Mohr) modifications, but in a more detailed and accurate manner; because the different frequencies, means, and asynchronous time variations and time shifts of the stress components are taken into account as well.



It is evident that the  $\Sigma_a(R = -1)$  and  $\Gamma(\sigma_m, \sigma_u)$  are different for the fiber and resin (matrix) phases; so that, Eqn. (13) must be checked for both phases. In other words, Eqn. (13) may be used for fiber breakage and matrix cracking fatigue failure checking, if local phase strengths are employed, as explained in the next sections. The fatigue strengths may be related to the number of cycles as follows:

$$\Sigma_{a1}(R = -1) = \Sigma_1^* N_{\sigma_1}^{-m_{\sigma_1}^{-1}}, \quad \Sigma_{a1}(R = -1) = \Sigma_2^* N_{\sigma_2}^{-m_{\sigma_2}^{-1}}, \quad T_a(R = -1) = T^* N_{\tau}^{-m_{\tau}^{-1}} \quad (14)$$

Therefore, Eqn. (13) may be rewritten as:

$$\left[ \frac{\sigma_{a1}}{\Sigma_1^* N_{\sigma_1}^{-m_{\sigma_1}^{-1}} \Gamma_{\sigma_1}(\sigma_{m1}, \sigma_{u1})} \right]^2 + \left[ \frac{\sigma_{a2}}{\Sigma_2^* N_{\sigma_2}^{-m_{\sigma_2}^{-1}} \Gamma_{\sigma_2}(\sigma_{m2}, \sigma_{u2})} \right]^2 + \\ + \left[ \frac{(\tau_{12})_a}{T^* N_{\tau}^{-m_{\tau}^{-1}} \Gamma_{\tau_{12}}(\tau_m, \tau_u)} \right]^2 - \frac{\sigma_{a1} \sigma_{a2}}{\Sigma_1^* \Sigma_2^* N_{\sigma_1}^{-m_{\sigma_1}^{-1}} N_{\sigma_2}^{-m_{\sigma_2}^{-1}} \Gamma_{\sigma_1}(\sigma_{m1}, \sigma_{u1}) \Gamma_{\sigma_2}(\sigma_{m2}, \sigma_{u2})} = 1 \quad (15)$$

where the fatigue strengths associated with a single half-cycle may be denoted by Basquin's standard notations:

$$\Sigma^* \equiv \sigma'_j; \quad T^* \equiv \tau'_f \quad (16)$$

Despite the common way of description of the fatigue life, using the number of cycles as a measure of the life of the component is a non-professional act. Because this number neither is identical for all the stress components in random loading nor the ordinary customers can count the cycles of the stress components to check whether the component failure is imminent or not. For example, in automotive design, the traveling mileages can much successfully be adopted in this regard. On the other hand, the following number of cycles ratios may be defined based on the stochastic histograms of the different stress components:

$$\lambda_{\sigma} = \frac{N_{\sigma_2}}{N_{\sigma_1}} = \frac{\Delta t|_{\sigma_2}}{\Delta t|_{\sigma_1}}; \quad \lambda_{\tau} = N_{\tau} / N_{\sigma_1} = \frac{\Delta t|_{\sigma_1}}{\Delta t|_{\tau}} \quad (17)$$

where e.g.,  $\Delta t|_{\tau}$  is the time spent by a one-half cycle of  $\tau$  and so on. These ratios indicate what would be the number of cycles of the other stress components when the base stress component lasts for an arbitrary  $N_{\sigma_1}$  number of cycles. Subsequently, Eqn. (15) may be rewritten as:

$$\left[ \frac{\sigma_{a1}}{\Sigma_1^* N_{\sigma_1}^{-m_{\sigma_1}^{-1}} \Gamma_{\sigma_1}(\sigma_{m1}, \sigma_{u1})} \right]^2 + \left[ \frac{\sigma_{a2}}{\Sigma_2^* \lambda_{\sigma}^{-m_{\sigma_2}^{-1}} N_{\sigma_1}^{-m_{\sigma_2}^{-1}} \Gamma_{\sigma_2}(\sigma_{m2}, \sigma_{u2})} \right]^2 + \\ + \left[ \frac{(\tau_{12})_a}{T^* \lambda_{\tau}^{-m_{\tau}^{-1}} N_{\sigma_1}^{-m_{\tau}^{-1}} \Gamma_{\tau_{12}}(\tau_m, \tau_u)} \right]^2 - \frac{\sigma_{a1} \sigma_{a2}}{\Sigma_1^* \Sigma_2^* N_{\sigma_1}^{-m_{\sigma_1}^{-1}} N_{\sigma_2}^{-m_{\sigma_2}^{-1}} \lambda_{\sigma}^{-m_{\sigma_2}^{-1}} \Gamma_{\sigma_1}(\sigma_{m1}, \sigma_{u1}) \Gamma_{\sigma_2}(\sigma_{m2}, \sigma_{u2})} = 1 \quad (18)$$

Eqn. (18) is an implicit form of the associated 2D S-N curve that incorporates influences of the different stress ratios, cycle ratios for identical time intervals, mean stresses, and material degradation. Therefore, the number of cycles to failure of the base stress component ( $N_{\sigma_1}$ ) may be readily determined by utilizing the information of the nested rain-flow counting data and the initial material properties of the material, including the fatigue strengths associated with  $R = -1$ . Now that the



damage equivalence has been established for a single one-half cycle of the base stress component, the accumulated fatigue damage may be determined based on the Miner-Palmgren rule:

$$D = \sum_{i=1} \frac{0.5}{N_{\sigma_i}} \quad (19)$$

#### *The complex equivalent-stress-based criterion*

To trace the instantaneous fatigue damages, another criterion may also be proposed. The static version of the failure criterion (9) may be rewritten in different ways:

$$\begin{aligned} & \left( \frac{\sigma_1}{X} \right)^2 + \left( \frac{\sigma_2}{Y} \right)^2 + \left( \frac{\tau}{S} \right)^2 - \frac{\sigma_1 \sigma_2}{XY} = 1 \Rightarrow \begin{cases} \left( \sigma_1 \right)^2 + \left( \frac{X}{Y} \sigma_2 \right)^2 + \left( \frac{X}{S} \tau \right)^2 - \frac{X}{Y} \sigma_1 \sigma_2 = X^2 \\ \left( \frac{Y}{X} \sigma_1 \right)^2 + \left( \sigma_2 \right)^2 + \left( \frac{Y}{S} \tau \right)^2 - \frac{Y}{X} \sigma_1 \sigma_2 = Y^2 \\ \left( \frac{S}{X} \sigma_1 \right)^2 + \left( \frac{S}{Y} \sigma_2 \right)^2 + \left( \tau \right)^2 - \frac{S^2}{XY} \sigma_1 \sigma_2 = S^2 \end{cases} \end{aligned} \quad (20)$$

However, this criterion may be enhanced further. To extend the conclusion of the author in Eqn. (20) to dynamic loading cases, this conclusion is first rewritten in the following more general form:

$$\alpha(\sigma_1)^2 + \beta(\sigma_2)^2 + \delta(\tau)^2 - \sqrt{\alpha\beta}\sigma_1\sigma_2 = 1 \quad (21)$$

Therefore, the following equivalent stresses may be proposed in directions parallel and transverse to the fibers:

$$(\sigma)_{eq}^2 = \left[ (\sigma_1)^2 + \beta^*(\sigma_2)^2 + \delta^*(\tau)^2 - \sqrt{\beta^*}\sigma_1\sigma_2 \right] \quad (22)$$

$$(\sigma)_{eq}^2 = \left[ (\sigma_2)^2 + \hat{\alpha}(\sigma_1)^2 + \hat{\delta}(\tau)^2 - \sqrt{\hat{\alpha}}\sigma_1\sigma_2 \right] \quad (23)$$

$$(\tau)_{eq}^2 = \left[ (\tau)^2 + \bar{\alpha}(\sigma_1)^2 + \bar{\beta}(\sigma_2)^2 - \sqrt{\bar{\alpha}\bar{\beta}}\sigma_1\sigma_2 \right] \quad (24)$$

where the nine coefficients indicated by “\*”, “~”, and “=” have to be related to appropriate fatigue strengths, as explained later. Eqn. (22) may be employed to check the failure due to the breakage of the fibers whereas Eqns. (23) and (24) may be used to check the matrix cracking and the shear failure, e.g., at the interfaces between layers or due to the relative slippage between the fiber and matrix, respectively. To explain the procedure of determination of coefficients of Eqns. (22) to (24), we now process Eqn. (22). A similar procedure holds for Eqns. (23) and (24). This equation has to meet the following uniaxial test results, at the fatigue failure, to ensure that its definition is valid for all loading conditions:

$$\begin{aligned} \sigma_2, \tau = 0 : \quad & (\sigma_{eq})_a = \sigma_{a1} = \Sigma_{a1}(N_{\sigma_1}, R_{\sigma_1}) \\ \sigma_1, \tau = 0 : \quad & (\sigma_{eq})_a = \sqrt{\beta^*}\sigma_{a2} = \sqrt{\beta^*}\Sigma_{a2}(N_{\sigma_2}, R_{\sigma_2}) \\ \sigma_1, \sigma_2 = 0 : \quad & (\sigma_{eq})_a = \sqrt{\delta^*}\tau_a = \sqrt{\delta^*}T_a(N_{\tau}, R_{\tau}) \end{aligned} \quad (25)$$

Comparing the second and third equations with the first relation of Eqn. (25) leads to:



$$\begin{aligned}\sqrt{\beta^*} &= \Sigma_{a1}(N_{\sigma_1}, R_{\sigma_1}) / \Sigma_{a2}(N_{\sigma_2}, R_{\sigma_2}) \\ \sqrt{\delta^*} &= \Sigma_{a1}(N_{\sigma_1}, R_{\sigma_1}) / T_a(N_{\tau}, R_{\tau})\end{aligned}\quad (26)$$

Therefore, according to Eqns. (22) and (26), one may deduce that:

$$\sigma_{eq}(t) = \sqrt{\left[ \sigma_1(t) \right]^2 + \left\{ \frac{\Sigma_{a1}|_{R_{\sigma_1}=-1} \Gamma_{\sigma_1}(\sigma_m, \sigma_u)}{\Sigma_{a2}|_{R_{\sigma_2}=-1} \Gamma_{\sigma_2}(\sigma_m, \sigma_u)} \sigma_2(t) \right\}^2 + \left\{ \frac{\Sigma_{a1}|_{R_{\sigma_1}=-1} \Gamma_{\sigma_1}(\sigma_m, \sigma_u)}{T_a|_{R_{\tau}=-1} \Gamma_{\tau_{12}}(\tau_m, \tau_u)} \tau(t) \right\}^2 + \frac{\Sigma_{a1}|_{R_{\sigma_1}=-1} \Gamma_{\sigma_1}(\sigma_m, \sigma_u)}{\Sigma_{a2}|_{R_{\sigma_2}=-1} \Gamma_{\sigma_2}(\sigma_m, \sigma_u)} \sigma_1(t) \sigma_2(t)} \quad (27)$$

The time history of  $\sigma_{eq}(t)$  stress has to be plotted and the contents of the cycle histograms may be determined based on the Rainflow procedure; so that Miner's damage accumulation rule can be applied to the stochastic time history sample to evaluate the resulting fatigue damage:

$$D = \sum_{i=1} (n_i)_{eq} \quad (28)$$

where

$$N_{\sigma_{eq}} = \left\{ \frac{\Sigma_1^* \Gamma[(\sigma_m)_{eq}, R_{\sigma_{eq}}, \sigma_u]}{(\sigma_a)_{eq}} \right\}^{m_{\sigma_1}} \quad (29)$$

$(n_i)_{eq}$  is the number of cycles associated  $N_{\sigma_{eq}}$  for the  $i$ th Rainflow cycle counting stage of the histogram of the equivalent stress.

To check the matrix failure, one may start from Eqn. (23), expressing all fatigue strengths in terms of  $Y$  instead of  $X$ . Using a procedure similar to that led to Eqn. (27), the following equivalent stress expression may be proposed for checking the matrix cracking:

$$\sigma_{eq}(t) = \sqrt{\left[ \sigma_2(t) \right]^2 + \left\{ \frac{\Sigma_{a2}|_{R_{\sigma_2}=-1} \Gamma_{\sigma_2}(\sigma_m, \sigma_u)}{\Sigma_{a1}|_{R_{\sigma_1}=-1} \Gamma_{\sigma_1}(\sigma_m, \sigma_u)} \sigma_1(t) \right\}^2 + \left\{ \frac{\Sigma_{a2}|_{R_{\sigma_2}=-1} \Gamma_{\sigma_2}(\sigma_m, \sigma_u)}{T_a|_{R_{\tau}=-1} \Gamma_{\tau_{12}}(\tau_m, \tau_u)} \tau(t) \right\}^2 + \frac{\Sigma_{a2}|_{R_{\sigma_2}=-1} \Gamma_{\sigma_2}(\sigma_m, \sigma_u)}{\Sigma_{a1}|_{R_{\sigma_1}=-1} \Gamma_{\sigma_1}(\sigma_m, \sigma_u)} \sigma_1(t) \sigma_2(t)} \quad (30)$$

Similarly, starting from Eqn. (24), shear failure may be checked by using the following equivalent stress expression:

$$\tau_{eq}(t) = \sqrt{\left\{ \frac{T_a|_{R_{\tau}=-1} \Gamma_{\tau_{12}}(\tau_m, \tau_u)}{\Sigma_{a1}|_{R_{\sigma_1}=-1} \Gamma_{\sigma_1}(\sigma_m, \sigma_u)} \sigma_1(t) \right\}^2 + \left\{ \frac{T_a|_{R_{\tau}=-1} \Gamma_{\tau_{12}}(\tau_m, \tau_u)}{\Sigma_{a2}|_{R_{\sigma_2}=-1} \Gamma_{\sigma_2}(\sigma_m, \sigma_u)} \sigma_2(t) \right\}^2 + \tau^2(t) + \frac{\left\{ T_a|_{R_{\tau}=-1} \Gamma_{\tau_{12}}(\tau_m, \tau_u) \right\}^2}{\Sigma_{a1}|_{R_{\sigma_1}=-1} \Sigma_{a2}|_{R_{\sigma_2}=-1} \Gamma_{\sigma_1}(\sigma_m, \sigma_u) \Gamma_{\sigma_2}(\sigma_m, \sigma_u)} \sigma_1(t) \sigma_2(t)} \quad (31)$$

So that, Eqn. (28) may be replaced by:



$$D = \sum_{i=1}^n \frac{(n_i)_{eq}}{N_{\tau_{eq}}} N_{\tau_{eq}} ; \quad N_{\tau_{eq}} = \left\{ \frac{\Sigma_1^* \Gamma \left[ (\tau_m)_{eq}, R_{\tau_{eq}}, \tau_u \right]}{(\tau_a)_{eq}} \right\}^{m_\tau} \quad (32)$$

## THE PROPOSED GENERALIZED LAMINA- AND PHASE-BASED PROGRESSIVE DAMAGE MODELS

The available progressive damage models have generally employed homogenization laws to replace the multi-phase orthotropic composite mixture with a homogeneous equivalent single-phase material. Therefore, the extracted stress components can be assigned to neither the fiber phase nor the matrix resin phase. To trace the progression of the fatigue damage within the different plies, in the form of the resin cracking, fiber-resin debonding, and fiber breakage more accurately, two quite different approaches/logics are proposed and implemented here:

- a) The lamina-based damage analysis,
- b) The phase-based (RVE-based) damage tracing.

### *The lamina-based progressive damage model*

The lamina-based approach of damage progression tracing may be coupled successfully with the equivalent damage criterion. In this regard, the stresses must be transformed from the geometric to principal directions of the material of each lamia. The localized damages can then be predicted based on the information, such as the S-N and T-N diagrams, of the ply under consideration.

The stress component computed by the finite element analysis code in the geometric coordinates may be related to the stresses in the material coordinates through the following relation:

$$\begin{Bmatrix} \sigma_1 \\ \sigma_2 \\ \tau_{12} \end{Bmatrix} = \mathbf{T} \begin{Bmatrix} \sigma_x \\ \sigma_y \\ \tau_{xy} \end{Bmatrix} \quad (33)$$

where

$$\mathbf{T} = \begin{bmatrix} \cos^2 \theta & \sin^2 \theta & \sin(2\theta) \\ \sin^2 \theta & \cos^2 \theta & -\sin(2\theta) \\ -\sin \theta \cos \theta & \sin \theta \cos \theta & \cos(2\theta) \end{bmatrix} \quad (34)$$

$\mathbf{T}$  is the so-called transformation matrix and  $\theta$  is the fibers angle with the first geometric axis.

### *The phase-based (RVE-based) progressive damage model*

Here, a generalization to the traditional approach of the representative volume element (RVE) is suggested and employed. Since each layer is randomly occupied by the fiber and resin phases, from the microscopic point of view, it is recommended to extract the histograms of the strain components instead of the stress components based on the meso-inspired micromechanical laws first. A typical RVE of the principal coordinates of the material of a specific lamina may be chosen as Fig. 2. This RVE-based model can be coupled with the second fatigue failure model. The stress components in the principal directions of the material can be computed from Eqn. (35), for each RVE. Although the possibility of the slippage of the fiber relative to the matrix may easily be checked later, when this slippage does not exist one may write:

$$\begin{Bmatrix} \varepsilon_1 \\ \varepsilon_2 \\ \gamma_{12} \end{Bmatrix}_{fiber} = \begin{Bmatrix} \varepsilon_1 \\ \varepsilon_2 \\ \gamma_{12} \end{Bmatrix}_{resin} \Rightarrow \begin{Bmatrix} \sigma_1 \\ \sigma_2 \\ \tau_{12} \end{Bmatrix}_{fiber/resin} = \mathbf{Q}_{fiber/resin} \begin{Bmatrix} \varepsilon_1 \\ \varepsilon_2 \\ \gamma_{12} \end{Bmatrix}_{fiber/resin} \quad (35)$$



where  $\mathbf{Q}$  is the stiffness matrix of the phase under consideration. Therefore, the local stresses may be computed whether the spatial material point is occupied by the fibers or resin. Thus, these actual phase stresses may be used for tracing the local damage progression [18,19] (e.g., fiber/resin breakage/crack) in both the fiber and resin phases, in contrast to the stresses that may be obtained from a homogenized model. As the previous approach, this approach can be utilized to not only prediction of the first failure onset but also for tracing the propagation of the fatigue damage and tracing the next failures. As Fig. 2 implies, the resulting stresses may be used to trace the relevant phase failure (resin cracking, fiber breakage, and resin-matrix separation/debonding) by using the relevant S-N or T-N diagram, as outlined by the second criterion.

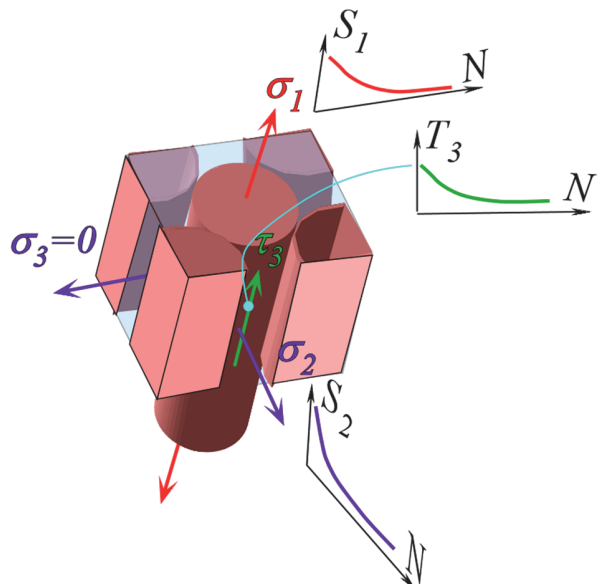


Figure 2: A representative unit cell for utilizing the phase-based fatigue criteria. The transverse normal stress of the thin structures may be set equal to zero.

## REVISITING THE RESIDUAL STIFFNESS AND MATERIAL PROPERTIES DEGRADATION CONCEPTS

Post et al. [20] presented a comprehensive literature survey on the residual-strength-based fatigue theories field of the composites. However, the concept of residual strength is an automatic outcome of damage law (e.g., Miner's law).

The attempts spent to define relations for the residual fatigue strength have led to simple and approximate equations that have ignored many complexities of the fatigue damage phenomena. The worst is that due to the huge band of the scatter of the fatigue test results, such relations cannot be determined accurately. Therefore, instead of using approximate equations for the residual strength, the direct usage of Miner's rule is recommended and implemented by the author.

Stiffness degradation is not restricted to composites but no such concept has been employed e.g., for life assessment of the metals/alloys [21-24]. Some researchers have stated that almost no indications of the elastic moduli degradation may be noted for the fibers and the small stiffness degradation of the resin matrix mainly happens in the last 20-30 percent or even, the last cycles [16] of the fatigue life. Some researchers considered no degradation in the material properties but showed excellent agreement with the experimental results [3,25,26]. Some others have claimed that due to the huge scatter in test data, it seems meaningless to predict the residual strength degradation or degradation in the material properties, especially when the fiber breakage is the dominant fracture mode [4]. In the present research, due to the mentioned difficulties in the experimental determination of the degradation in the material properties of the resin phase, the following standard form of normalized function of gradual stiffness degradation [10] is modified:

$$E(\sigma, n, \dot{\varepsilon}) = \left[ 1 - \left( \frac{\log(n) - \log(0.25)}{\log(N_f) - \log(0.25)} \right)^g \right]^{\mu} \left( E_0 - \frac{\sigma}{\varepsilon_{f0}} \right) + \frac{\sigma}{\varepsilon_{f0}} \quad (36)$$



where  $E_0$  and  $\varepsilon_{f0}$  are the initial elastic modulus and the initial static failure strain, respectively.  $\vartheta$  and  $\mu$  are curve fitting material properties. As explained later, the elastic modulus is a strain-dependent quantity as well. For this reason, Eqn. (36) may be modified in the following form;

$$E(R, \sigma, n, \dot{\varepsilon}) = \left\{ \left[ 1 - \left( \frac{\log(n) - \log(0.25)}{\log(N_f) - \log(0.25)} \right)^{\vartheta} \right]^{\mu} \left( E_0 - \frac{\sigma}{\varepsilon_{f0}} \right) + \frac{\sigma}{\varepsilon_{f0}} \right\} f(\dot{\varepsilon}) \quad (37)$$

where the strain-rate-dependence function  $f(\dot{\varepsilon})$  is defined later in Tab. 2. for these composites. The effects of the strain-rate-dependence on the results are much more significant than those of the stiffness-degradation itself, as may be discussed later.

## EXPERIMENTAL IDENTIFICATIONS OF THE MATERIALS AND THE STRAIN-RATE-DEPENDENCE OF THE MATERIAL PROPERTIES

### *Important declarations*

**I**t should be declared that due to the vast variety of the required experimental data, some of the experimental materials identification activities were accomplished through testing requests to some automotive materials and components testing companies whereas some experiments were performed through testing orders to universities/industries fatigue and fracture research laboratories. The fatigue tests of the full vehicle and some tests regarding the fatigue strengths were accomplished by either the automotive materials, systems, and components testing companies, or by the facilities prepared by the testing team of the vehicle redesign project, under the author's supervision. The gathered database may be published in a series of full-length papers. But the ownership of the various data has not been resolved yet and the contributions are not assigned in those papers. For this reason, only the results that may be derived based on mainly three-point regressions are reported in the present article.

### *The experimental material identification results*

The fatigue tests were performed for components made of E-Glass/Epoxy (E-Glass fiber with CY225 epoxy resin and HY225 hardener) and Carbon/Epoxy (T300/LY556 and HY5200 hardener) materials whose preliminary material properties are:

E-Glass/Epoxy:  $\nu_{12} = 0.22$ ,  $\rho = 1830 \text{ (kg/m}^3\text{)}$

Carbon/Epoxy:  $\nu_{12} = 0.3$ ,  $\rho = 1600 \text{ (kg/m}^3\text{)}$

The preliminary static properties and strengths of the materials are extracted based on the ASTM standards. The static strengths, elastic moduli, and Poisson's ratios are determined according to the ASTM D3039 standard, whereas the shear strengths and the shear elastic moduli are extracted according to ASTM D3518 standard. These quantities constitute the limiting values for those of the fatigue strengths and stiffnesses. The results are extracted in the  $23 \pm 3^\circ C$  ambient temperature and  $50 \pm 10\%$  humidity. The static tensile tests were accomplished at 2mm/min velocity and the standard strain rate of  $0.01 \text{ min}^{-1}$ .

The fatigue test, especially, the high strain rate fatigue tests, was performed using Instron and Dartec Servo-hydraulic Fatigue Testing Machines.

The material properties in directions parallel (denoted by 1) and perpendicular to fibers (indicated by 2) may be derived based on proper micromechanical homogenization models, e.g.:

$$E_1 = E_f V_f + E_m V_m; \quad E_2 = \frac{E_f E_m}{E_f V_m + E_m V_f}; \quad \nu_{12} = \nu_f V_f + \nu_m V_m; \quad G_{12} = \frac{G_f G_m}{G_f V_m + G_m V_f} \quad (38)$$

where the subscripts  $f$  and  $m$  denote the fiber and matrix, respectively.



The strain-rate-dependence of a representative elastic modulus  $P$  (e.g.,  $E_1$ ) may be expressed as follows, according to the previous experiments of the author [27]:

$$P(\dot{\varepsilon}) = \mathcal{A} + \mathcal{B}\dot{\varepsilon}^\lambda \quad (39)$$

where,  $\mathcal{A}$ ,  $\mathcal{B}$ , and  $\lambda$  are material constants whose values are given in Tab. 1 for the E-Glass/Epoxy and Carbon/Epoxy composites and  $\dot{\varepsilon}$  is the strain rate in the fiber direction.

Material	Material constant	$E_1$ (GPa)	$E_2$ (GPa)	$G_{12}$ (GPa)
E-Glass/Epoxy	$\mathcal{A}$	37.2	10.037	4.919
	$\mathcal{B}$	1.139	0.437	-0.9408
	$\lambda$	0.276	0.2624	0.0545
Carbon/Epoxy	$\mathcal{A}$	120.7	7.93	5.5
	$\mathcal{B}$	3.691	0.345	-1.0519
	$\lambda$	0.276	0.2624	0.0545

Table 1: Material constants of the E-Glass/Epoxy and Carbon/Epoxy composites, for  $0.001 \leq \dot{\varepsilon} \leq 100 \text{ s}^{-1}$  [27].

On the other hand, for the RVE-based analyses, the strain-rate-dependence functions of the elastic moduli and the S-N diagrams of the individual phases are required. The explicit forms of these functions are listed in Tab. 2 for the employed E-Glass/Epoxy and Carbon/Epoxy composites. In Tab. 2,  $\dot{n}$  denotes the cycle per second quantity.

The strain rate  $\dot{\varepsilon}$  may be determined based on the time history of the strains in the fiber direction. In each time instant, the stresses associated with the strain-independent condition are determined first. Then, according to the resulting entire time histories of the stresses, the relevant complete set of the time histories of the strains and  $\dot{\varepsilon} = \Delta\varepsilon / \Delta t$  are determined for each time step.

Main composition	Material/phase	Elastic moduli strain-rate dependence function	Strain-rate dependence function of $\Sigma_a _{R_{\sigma_i}=-1}$
Glass/Epoxy	UD fiber, along the fibers	$f(\dot{\varepsilon}) = 1 + 0.025\dot{\varepsilon}^{0.197}$	$g(\dot{n}) = 1 + 0.092\dot{n}^{0.005}$
	Epoxy resin	$f(\dot{\varepsilon}) = 1 + 0.126\dot{\varepsilon}^{0.206}$	$g(\dot{n}) = 1 + 0.738\dot{n}^{0.04}$
	Lamina, along the fibers	According to Tab. 1	$g(\dot{n}) = 1 + 0.048\dot{n}^{0.02}$
	Lamina, across the fibers	According to Tab. 1	$g(\dot{n}) = 1 + 0.161\dot{n}^{0.01}$
Carbon/Epoxy	UD Fibers, along the fibers	$f(\dot{\varepsilon}) = 1 + 0.014\dot{\varepsilon}^{0.192}$	$g(\dot{n}) = 1 + 0.0063\dot{n}^{0.004}$
	Epoxy resin	$f(\dot{\varepsilon}) = 1 + 0.1184\dot{\varepsilon}^{0.202}$	$g(\dot{n}) = 1 + 0.706\dot{n}^{0.04}$
	Lamina, along the fibers	According to Tab. 1	$g(\dot{n}) = 1 + 0.013\dot{n}^{0.03}$
	Lamina, across the fibers	According to Tab. 1	$g(\dot{n}) = 1 + 0.11\dot{n}^{0.008}$

Table 2: Strain-rate-dependence of the S-N diagram (fatigue strengths associated with  $R=-1$ ) and the elastic moduli of the individual phases and the laminas.

Although a linear relation can be established between the logarithms of the stress amplitude and the number of cycles [i.e.,  $\log(N) = a - b \cdot \log(\Sigma_a|_{R_{\sigma_i}=-1})$ ], a semi-logarithmic relation has been extensively used for the composite materials [14,17]:

$$\frac{S}{S_0} = a - b \cdot \log(N) \quad (40)$$

where  $S_0$  is the fatigue strength associated with one-cycle fatigue life ( $R = -1$ ). For small strain rates, the HCF region of the S-N curves associated with the three stress components of the E-Glass/Epoxy may be presented as:

$$\begin{aligned} \left[ \Sigma_{a1}(n_{\sigma_1}, N_{\sigma_1}) \right]_{R_{\sigma_1}=-1} &= 900 - 92.6 \times \log(N) \\ \left[ \Sigma_{a2}(n_{\sigma_2}, N_{\sigma_2}) \right]_{R_{\sigma_2}=-1} &= 61.2 - 4.5 \times \log(N) \\ \left[ T_a(n_{\tau}, N_{\tau}) \right]_{R_{\tau}=-1} &= 53.7 - 6.4 \times \log(N) \end{aligned} \quad (41)$$

On the other hand, the fatigue strengths associated with the three stress components of the employed Carbon/Epoxy may be introduced as:

$$\begin{aligned} \left[ \Sigma_{a1}(n_{\sigma_1}, N_{\sigma_1}) \right]_{R_{\sigma_1}=-1} &= 2008 - 240.48 \times \log(N) \\ \left[ \Sigma_{a2}(n_{\sigma_2}, N_{\sigma_2}) \right]_{R_{\sigma_2}=-1} &= 132 - 8.16 \times \log(N) \\ \left[ T_a(n_{\tau}, N_{\tau}) \right]_{R_{\tau}=-1} &= 103 - 12.8 \times \log(N) \end{aligned} \quad (42)$$

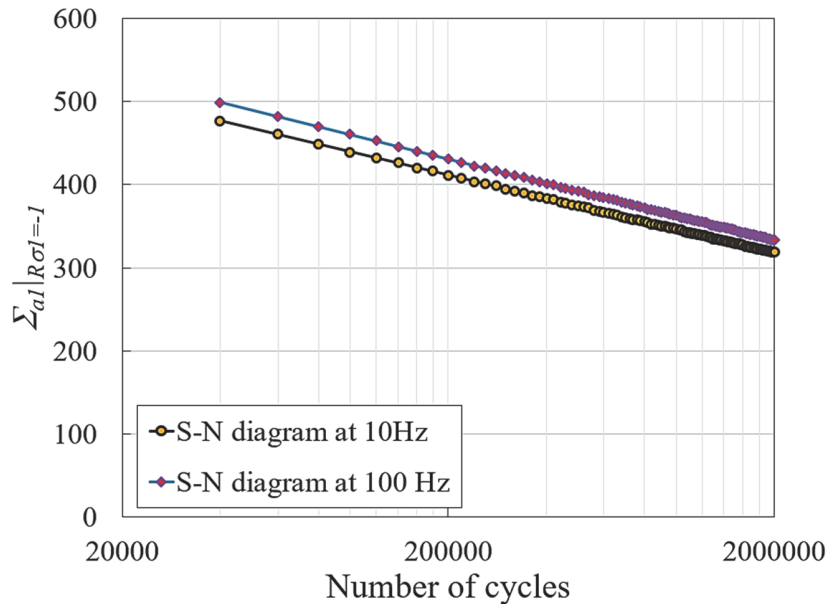


Figure 3: Influence of the loading rate on the S-N diagram of the employed E-Glass/Epoxy.

Eqns. (41) and (42) have to be multiplied by the strain-rate-dependence functions of Tab. 2. For example, for the employed E-Glass/Epoxy material one has:

$$\left[ \Sigma_{a1}(n_{\sigma_1}, N_{\sigma_1}) \right]_{R_{\sigma_1}=-1} = [900 - 92.6 \times \log(N)] (1 + 0.0048 \dot{n}^{0.02})$$



$$\left[ \Sigma_{\alpha 2}(n_{\sigma_2}, N_{\sigma_2}) \right]_{R_{\sigma_2}=-1} = [61.2 - 4.5 \times \log(N)](1 + 0.0161\dot{n}^{0.01}) \quad (43)$$

$$\left[ T_a(n_{\tau}, N_{\tau}) \right]_{R_{\tau}=-1} = [53.7 - 6.4 \times \log(N)](1 + 0.0161\dot{n}^{0.01})$$

Eqns. (41) to (43) are valid for the high-cycle domain only. For a better imagination, the HCF S-N diagrams of the employed E-Glass/Epoxy lamina are plotted in Fig. 3, for  $\dot{n} = 10$  and 50 Hz.

## RESULTS AND DISCUSSIONS

### Overview

The following two main comparative studies are accomplished in this section:

- (i) The proposed fatigue criteria are implemented to a rectangular composite strip with a complicated stacking sequence and the obtained theoretical results are compared with the experimental ones extracted by the author.
- (ii) The complete progressive damage fatigue life assessment algorithm is implemented to a finite element model of a realistic composite chassis frame of a recently redesigned SUV car under realistic random road inputs and the results are compared with the experimental results extracted from the four-poster durability tests of the SUV.

### The stochastic histogram of the road inputs

Since the road inputs have a random nature, the representative road histogram should be determined based on field measurements, based on the applicability percent. The stochastic sample of the time history must have the same mean and standard deviation of the whole time history of inputs of the road. Applicability percent of the redesigned/modified SUV may be categorized as:

- 50% mileage over the type B (good) roads with an average speed of 72 km/h,
- Traveling on 35% of the road length on type D (poor) roads with an average speed of 36 km/h.
- 15% of the length of the road comprises roads of type F (rough) with an average speed of 18 km/h.

The length of the stochastic road is chosen as 100m. The road inputs imposed on the right and left axles of the front and rear tires of the vehicle in GVW (gross vehicle weight) conditions are illustrated in Fig. 4. It is obvious that the inputs of the rear tires are identical to those of the front tires but with a specific time phase shift that depends on the vehicle's speed.

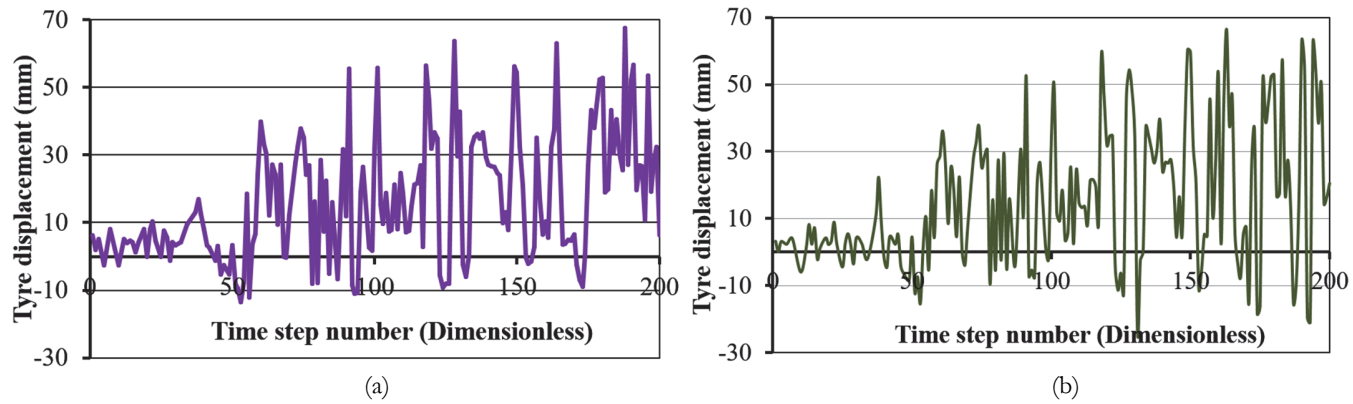


Figure 4: The representative stochastic time histories of the vertical inputs of the: (a) left and (b) right front tires.

### The first verification of the predictions of the two fatigue criteria

The first verification of the predictions of the proposed fatigue criteria has been accomplished by comparing the results of a multi-layer E-Glass/Epoxy strip. Dimensions of the plate are  $1000 \times 70 \times 15$  mm and a  $[\pm 45^\circ, 0^\circ]_4; \pm 45^\circ$  layup. The time histories shown in Fig. 4 are imposed as transverse loads, each force on distinct specimens, at the mid-span section. The schematic of the employed Instron Hydropuls test machine is demonstrated in Fig. 5. Four specimens were tested for each load entry.

The obtained theoretical predictions of the two categories of the proposed criteria are compared in Tab. 4 with the experimental results, for each loading entry. Since four specimens were used to extract the results for each entry, the predicted to experimental fatigue life ratios are plotted in Fig. 6. This figure implies that the predicted fatigue lives (in terms of kilometers of traveling) are in excellent agreement with the experimental results. Since generally, the fatigue life is proportional to the sixth to eighth power of the stresses, even a 200% discrepancy between the predicted and experimental fatigue lives may be regarded as a good estimation. However, the discrepancies between the present theoretical and experimental results are much less. Comparing the results of the proposed criteria in Fig. 6 shows that predictions of the effective-stress-based category of the criteria lead to a slightly lower mean discrepancy. Tab. 3 and Fig. 6 report the strain-rate-independent results as well. Our stress analysis results showed that the stresses associated with the strain-rate-dependent results are larger (up to 10%) than those of the strain-rate-independence assumption. For this reason, the fatigue lives associated with the strain-rate-dependent materials are slightly higher. It is the first time that the magnitudes of the possible discrepancy between the strain-rate-dependent and strain-rate-independent results are reported. The mean deviation of the strain-rate-independent results relative to the experimental results is about 60% which is higher than those of the strain-rate-dependent results. It is worth mentioning that the longitudinal and transverse matrix cracks may appear before the fiber breakage. However, due to safety issues, only the fiber breakage was detectable. Hence, the relevant theoretical damage results were considered, as well.

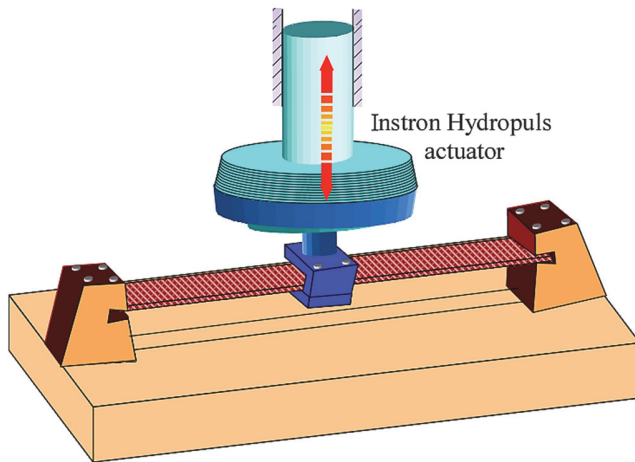


Figure 5: The schematic of the fatigue testing machine for the first verification test.

Load histogram correspondence	Strain-rate dependence	RVE-phase-based criterion	Lamina-based criterion	Experimental (4 specimens for each entry)
Front left tire	Considered	64183	59216	85993.5779 105439.439
	Ignored	89211	76926	113984.596 45130.2288
Front right tire	Considered	58274	55769	78566.0314 96176.2803
	Ignored	78734	73564	103906.3249 36966.8386

Table 3: A comparison among predictions of the proposed criteria and the experimental results, for the load histograms of the left and right front tires shown in Fig. 4.

#### *The FE model of the composite chassis frame*

The full finite element model of the composite chassis frame required for the second verification study is shown in Fig. 7 in conjunction with the full model of the SUV vehicle.

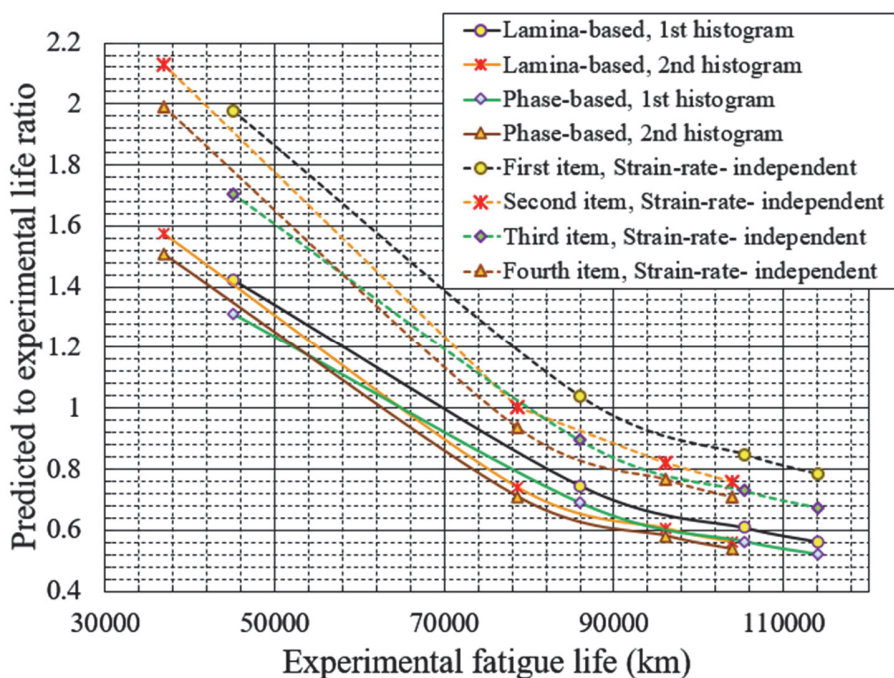


Figure 6: A comparison between the predicted to experimental fatigue life ratios of the proposed fatigue criteria associated with the load histograms of the: (1) left and (2) right front tires. Both strain-rate-dependent and strain-rate-independent results are reported. The smoothed lines are connecting the results of the four specimens used for each load entry.

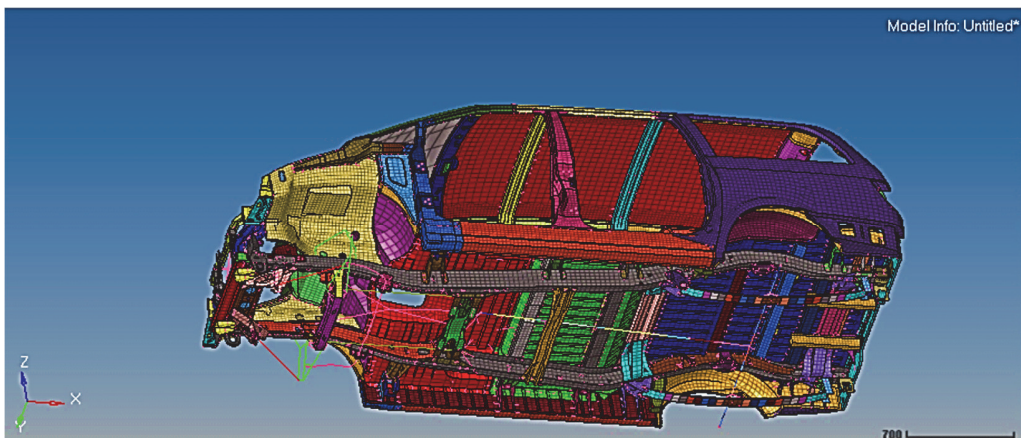


Figure 7: The composite chassis within the full SUV finite element analysis model.

The geometrical modeling has been accomplished in CATIA and Siemens PLM NX12 softwares. Meshing has been performed in Hypermesh 2019 and ANSA Beta CAE systems softwares. The chassis frame was meshed by 8-node quadratic S8R reduced-integration thick-shell elements. As Fig. 7 shows, all the components, assemblies, and subassemblies of the vehicle, even the suspension system, and the tires are included in the finite element model. Some of the model specifications are listed in Tab. 4.

To present a fair comparison, the thickness of the chassis is so chosen that almost identical strengths result under the static loading in comparison to the replaced metallic chassis. Based on the mentioned strategy, the thickness of the E-Glass/Epoxy and Carbon/Epoxy chassis frames are chosen as 8 and 6 millimeters, respectively. The chosen stacking sequence is a cross-ply one ([0/90/...]). The thickness of each layer is 0.5mm.

#### *The second more general verification study*

Now, the proposed criteria and the fatigue life assessment algorithms are implemented in the composite chassis frame. To this end, the time histories of the stress components are first determined in ABAQUS finite element analysis software, taking into account the strain-rate dependence of the material properties and using the stochastic sample of the load time

histories shown in Fig. 4. The time histories of the stress components have to be processed based on the proposed criteria to determine the critical elements which specify the fatigue life of the whole chassis frame. Some of the resulting stress analysis results [the equivalent stresses defined in Eqn. (27)] are depicted in Fig. 8.

Item	Quantity
GVW (Gross vehicle weight)	2650 kg
Front axle mass	95 kg
Rear-axle mass	125 kg
The front suspension stiffness	60200 N/m
The front suspension damping coefficient	11600 Ns/m
The rear suspension stiffness	74000 N/m
The rear suspension damping coefficient	1105 Ns/m
Vehicle's roll moment of the inertia	402 kgm <sup>2</sup>
Vehicle's pitch moment of the inertia	4308 kgm <sup>2</sup>
Vehicle's yaw moment of the inertia	3260 kgm <sup>2</sup>

Table 4: Some of the dynamic parameters of the full vehicle finite element model.

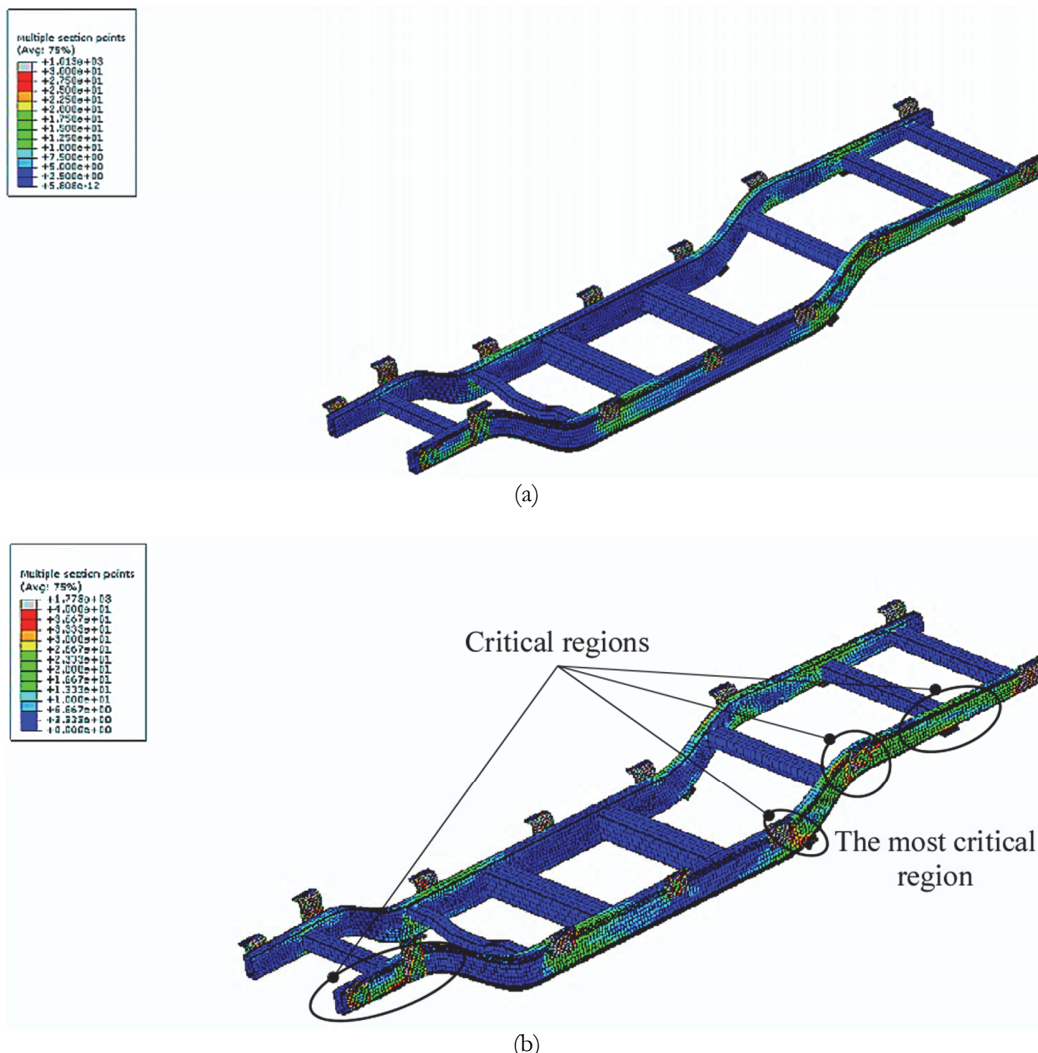


Figure 8: Typical contours of the  $\sigma_{eq}$  equivalent stress [Eqn. (27)] of the: (a) E-Glass/Epoxy and (b) Carbon/Epoxy chassis frames.

The most critical elements are shown in Fig. 8 and are located in a region ahead of the front mount of the rear leaf spring of the chassis. The obtained fatigue lives in terms of kilometers of traveling are reported in Tab. 5, for the main fatigue



failure modes, according to the two categories of the developed fatigue life assessment criteria. In this regard, the time histories of the road inputs shown in Fig. 4 are reproduced by a Servotest four-poster durability testing machine shown in Fig. 9. The empirical most critical region was coincident with those shown in Fig. 8. In Tab. 5, the theoretical fatigue lives are compared against the experimental results obtained by the author's industrial team. However, as mentioned before, the detection of the matrix crack initiation was not possible due to practical limitations. For this reason, only the fiber breakage results were comparable with the experimental results. The comparison is made in Tab. 6. Simultaneously, the strain-rate-independent theoretical results are compared with the experimental results.

Material	Criterion type		Damage type	Life
	First category	Second category		
E-glass/Epoxy	2.062		Matrix cracking initiation	1.821
			Fiber breakage initiation	2.731
			Full matrix cracking	3.796
			Full Shear cracking	4.301
Carbon/Epoxy	35.56		Matrix cracking initiation	29.67
			Fiber breakage initiation	38.01
			Full matrix cracking	47.605
			Full Shear cracking	54.85

Table 5: The computed fatigue lives (in terms of  $10^5$  kilometers) based on the two categories of the developed HCF criteria for the two types of composite chassis frames.

Fig. 10 that presents the ratio of the predicted theoretical results to the experimental results (each smooth line connects 3 experimental points of the same material) may be utilized to investigate the accuracy of the strain-rate-dependent (SRD) and strain-rate-independent (SRID) forms of the proposed criteria. As may readily be seen, in contrast to the fact that results of the present criteria are mathematically more accurate than the available criteria, the assumption of the strain-rate-independence of the material properties leads to considerable discrepancies relative to the experimental results. Indeed, the available criteria are special cases of the present generalized criteria. On the other hand, based on Tab. 6 and Fig. 10, when the strain-rate-dependence is considered, both categories of criteria lead to reliable results although the second category may reproduce the experimental results and the failure mode more accurately.



Figure 9: The employed Servotest four-poster testing facility.

Material	Criterion type		Experimental	
	First category	Second category	Raw result	Mean
E-glass/Epoxy	2.062	Strain-rate-dependent	2.731	1.6549
		Strain-rate-independent	7.592	2.5758 3.8872
Carbon/Epoxy	35.56	Strain-rate-dependent	38.01	15.2172
		Strain-rate-independent	95.21	22.6625 69.1638

Table 6: A comparison between the strain-rate-dependent and strain-rate-independent theoretical results (fatigue lives in terms of  $10^5$  kilometers) with the experimental results.

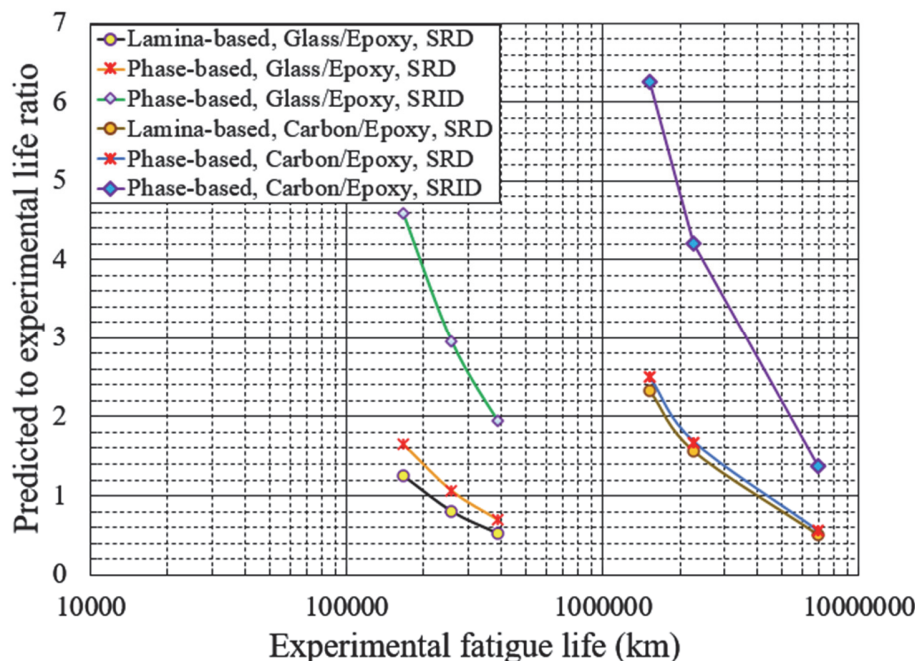


Figure 10: A comparison between the strain-rate-dependent (SRD) and strain-rate-independent (SRID) results of the theoretical results against the experimental results.

## CONCLUSIONS

Two of phase-based progressive-damaged-based HCF criteria, namely: (i) damage-based (lamina-based) and (ii) equivalent-stress-based (RVE/phase-based) criteria, are developed and extended for the multilayer composite components. While the first category of the criteria may be used mainly for detection of the fiber breakage and matrix cracking failure modes of the fiber-reinforced composites, the second framework enables detecting the fatigue failures at the phase scale; so that the shear fatigue failure may be detected as well. Predictions the two categories of criteria are compared against the experimental results under randomly varying loads and the following practical conclusions are obtained:

- An excellent concordance between the two categories of the fatigue criteria with the experimental results when the strain-rate dependence is considered.
- Due to the inherent higher resolution of the effective-stress-based category of criteria, it has reproduced the experimental results slightly more accurately.
- Due to using displacement-based inputs, the stresses associated with the strain-rate-dependent results are larger than those of the strain-rate-independence assumption. For this reason, the fatigue lives associated with the strain-rate-dependent materials are slightly higher.



- There are significant discrepancies between the theoretical strain-rate-independent results and the experimental results.
- The strain-rate-dependence functions affect the material properties, the resulting stresses, and the fatigue strengths (S-N and T-N diagrams).

## REFERENCE

- [1] Zhang, W., Zhou, Z., Scarpa, F., Zhao, S. (2016). A fatigue damage meso-model for fiber-reinforced composites with stress ratio effect. *Mater. Des.*, 107, pp. 212-20.
- [2] Lian, W., Yao, W. (2020). Fatigue life prediction of composite laminates by FEA simulation method. *Int. J. Fatigue*, 32, pp.123-133.
- [3] Quaresimin, M., Susmel, L., Talreja, R. (2010). Fatigue behaviour and life assessment of composite laminates under multiaxial loadings. *Int. J. Fatigue*, 32, pp. 2–16.
- [4] Nyman, T. (1996). Composite fatigue design methodology: a simplified approach. *Compos. Struct.* 35, pp. 183-194.
- [5] Naderi, M., Maligno, A.R. (2013). Finite element simulation of fatigue life prediction in carbon/epoxy laminates. *J. Compos. Mater.*, 47, pp. 475-84.
- [6] Dong, H., Li, Z., Wang J., Karihaloo, B.L. (2016). A new fatigue failure theory for multidirectional fiber-reinforced composite laminates with arbitrary stacking sequence. *Int. J. Fatigue*, 87, pp. 294-300.
- [7] Passipoularidis, V.A., Philippidis, T.P., Brondsted, P. (2011). Fatigue life prediction in composites using progressive damage modelling under block and spectrum loading. *Int. J. Fatigue*, 33, pp.132-44.
- [8] Carrella-Payan, D., Magneville, B., Hack, M., Lequesne, C., Naito, T., Urushiyama, Y., Yamazaki, W., Yokozeki, T., Van Paepegem, W. (2016). Implementation of fatigue model for unidirectional laminate based on finite element analysis: Theory and practice. *Frattura ed Integrità Strutturale*, 10 (38), pp. 184-190. DOI: 10.3221/IGF-ESIS.38.25.
- [9] Yang, Z., Pei, C., Yan, H., Long, L. (2020). Fatigue damage modeling of ceramic-matrix composites: A short review. *Mater. Design Process. Commun.*, 2 (2), e129, DOI: 10.1002/mdp.2129.
- [10] Vassilopoulos, A.P. (2020). The history of fiber-reinforced polymer composite laminate fatigue. *Int. J. Fatigue*, 105512.
- [11] Shariyat, M., Rahimi-Ghazat, M. (2020). Generalized 3D high cycle fatigue criteria for multiscale bridging-based progressive damage analysis of multilayer composite parts under random loads and material deterioration. *Fatigue Fract. Eng. Mater. Struct.*, 43, pp. 466–487.
- [12] Puck, A., Schurmann, H. (1998). Failure analysis of FRP laminates by means of physically based phenomenological models. *Compos. Sci. Tech.*, 58, pp. 1045-1067.
- [13] Kawai, M., Yano, K. (2016). Anisomorphic constant fatigue life diagrams of constant probability of failure and prediction of P-S-N curves for unidirectional carbon/epoxy laminates. *Int. J. Fatigue*, 83, pp. 323-34.
- [14] Mandell, J.F. (2004). DOE/MSU Composite Material Fatigue Database, Sandia National Laboratories, Albuquerque, NM.
- [15] Nijssen, R.P.L. (2006). Wind turbine in Wieringermeerpolder and constant life diagram of MD2 material. Netherlands: Gildeprint drukkerijen.
- [16] Reis, P.N., Ferreira, J.A., Costa, J.D., Richardson, M.O. (2009). Fatigue life evaluation for carbon/epoxy laminate composites under constant and variable block loading. *Compos. Sci. Tech.*, 69, pp.154-60.
- [17] DOE/MSU composite material fatigue database, Version 18.1, March 25, 2009.
- [18] Hack, M., Carrella-Payan, D., Magneville, B., Naito, T., Urushiyama, Y., Yamazaki, W., Yokozeki, T., Van Paepegem, W. (2018). A progressive damage fatigue model for unidirectional laminated composites based on finite element analysis: theory and practice. *Frattura ed Integrità Strutturale*, 46: pp. 54-61.
- [19] Tashkinov, M. (2019). Computational multi-scale analysis of simultaneous processes of delamination and damage accumulation in laminated composites. *Frattura ed Integrità Strutturale*, 13(49): p. 396.
- [20] Post, N.L., Lesko, J.J., Case, S.W. (2020). Residual strength fatigue theories for composite materials. In: *Fatigue life prediction of composites and composite structures*, pp. 77-97. Woodhead Publishing.
- [21] Shariyat, M. (2009). Three energy-based multiaxial HCF criteria for fatigue life determination in components under random non-proportional stress fields. *Fatigue Fract. Eng. Mater. Struct.*, 32, pp.785-808.
- [22] Shariyat, M. (2009). Two new multiaxial HCF criteria based on virtual stress amplitude and virtual mean stress concepts, for complicated geometries and random non-proportional loading conditions. *Trans. ASME, J. Eng. Mater. Technol.*, 131, 031014, pp. 1-13.



- 
- [23] Shariyat, M. (2010). New multiaxial HCF criteria based on instantaneous fatigue damage tracing in components with complicated geometries and random non-proportional loading conditions. *Int. J. Damage Mech.*, 19, pp. 659-690.
  - [24] Reza Kashyzadeh, K., Farrahi, G.H., Shariyat, M., Ahmadian, M.T. (2018). Experimental accuracy assessment of various high-cycle fatigue criteria for a critical component with a complicated geometry and multi-input random non-proportional 3D stress components. *Eng. Fail. Analysis*, 90, pp. 534-553.
  - [25] Zhou, S., Sun, Y., Guo, L. (2017). Random fatigue life prediction of carbon fibre-reinforced composite laminate based on hybrid time-frequency domain method. *Adv. Compos. Mater.*, 26, pp. 181-95.
  - [26] Brunbauer, J., Gaier, C., Pinter, G. (2015). Computational fatigue life prediction of continuously fibre reinforced multiaxial composites. *Compos. Part B*, 80, pp. 269-77.
  - [27] Shariyat, M., Niknami, A. (2016). Impact analysis of strain-rate-dependent composite plates with SMA wires in thermal environments: Proposing refined coupled thermoelasticity, constitutive, and contact models. *Compos. Struct.*, 136, pp. 191-203.